scientific reports

Check for updates

OPEN

The left ventricular mechanical dispersion as a marker of disease severity in transthyretin cardiac amyloidosis

Katarzyna Holcman[1,2,8]✉, Paweł Rubiś[1,8], Bogdan Ćmiel[3], Andrzej Ząbek[4,8], Krzysztof Boczar[4,8], Agnieszka Stępień-Wroniecka[1,5,8], Katarzyna Graczyk[1,5,8], Krystian Mróz[6,8], Ewa Dziewięcka[1,8], Winiarczyk Mateusz[1,5,8], Sylwia Szczepara[1,8], Maria Kurek[7], Karolina Gutkowska[7], Piotr Podolec[1,8] & Magdalena Kostkiewicz[1,2,8]

Transthyretin amyloidosis (ATTR) is a fatal disorder, thus early detection of cardiac involvement is crucial for improved clinical outcomes. This study investigated the utility of left ventricular (LV) speckle-tracking-derived mechanical dispersion as a potential marker for the assessment of cardiac amyloidosis (CA) in patients with ATTR and their first-degree relatives. This prospective, single-centre study enrolled 100 adults from 2020 to 2024 (ClinicalTrials NCT05814380). Participants underwent clinical assessment, genetic testing, and [^{99m}Tc]Tc-DPD SPECT/CT. Global longitudinal strain (GLS) and mechanical dispersion were evaluated using speckle-tracking echocardiography. Patients with ATTR CA exhibited significantly impaired GLS and increased mechanical dispersion ($p < 0.001$). Mechanical dispersion exhibited correlations with age, New York Heart Association class, LV mass index, E/E', LV ejection fraction, GLS, levels of N-terminal pro-brain natriuretic peptide and Perugini grade ($p < 0.05$ for all). In univariable Cox regression, mechanical dispersion (Hazard ratio (HR) = 1.03, 95% confidence intervals (CI) 1.01–1.06, $p = 0.004$), normalised to heart rate mechanical dispersion (HR = 1.43, 95% CI 1.14–1.81, $p = 0.002$) were significant predictors of all-cause mortality. In our study increased mechanical dispersion was associated with advanced disease stages and mortality. These findings suggest that it may serve as a marker of ATTR CA.

***Registration*: ClinicalTrials.gov Identifier: NCT05814380.**

Keywords Amyloidosis, ATTR, Mechanical dispersion, Speckle-tracking echocardiography

Transthyretin amyloidosis (ATTR) is a progressive and debilitating disease characterized by the deposition of misfolded transthyretin (TTR) protein in various organs, including the heart[1]. This cardiac involvement can lead to left ventricular (LV) dysfunction, conduction abnormalities, and arrhythmias, which can significantly impact patient outcomes[2,3]. Early detection of cardiac involvement is crucial for timely management and improving prognosis[4,5].

Speckle-tracking echocardiography (STE), a non-invasive imaging technique, has emerged as a valuable tool in the assessment of myocardial mechanics and the identification of subtle changes in cardiac function[6]. In the context of cardiac amyloidosis (CA), this technology has been employed to characterize the specific patterns of cardiac mechanics, revealing that patients with ATTR often exhibit impaired longitudinal, radial, and circumferential strain, as well as increased mechanical dispersion, when compared to healthy controls[7,8].

[1]Department of Cardiac and Vascular Diseases, Institute of Cardiology, Jagiellonian University Medical College, St. John Paul II Hospital, Krakow, Poland. [2]Department of Nuclear Medicine, St. John Paul II Hospital, Krakow, Poland. [3]Faculty of Applied Mathematics, AGH University of Krakow, Krakow, Poland. [4]Department of Electrocardiology, Jagiellonian University Medical College, St. John Paul II Hospital, Krakow, Poland. [5]Doctoral School of Medical and Health Sciences, Jagiellonian University Medical College, Krakow, Poland. [6]Department of Interventional Cardiology, Jagiellonian University Medical College, Institute of Cardiology St. John Paul II Hospital, Krakow, Poland. [7]Students Scientific Group of Cardiovascular Imaging, Department of Cardiac and Vascular Diseases, Jagiellonian University Medical College, Krakow, Poland. [8]St. John Paul II Hospital, Pradnicka 80, Krakow 31-202, Poland. ✉email: katarzyna.holcman@gmail.com

Mechanical dispersion, which quantifies the temporal heterogeneity of myocardial contraction, is a parameter of particular interest as it has been shown to be a sensitive indicator of cardiac dysfunction in various cardiomyopathies and may hold promise as a valuable tool for the early detection of CA[9].

These findings underscore the potential of STE as a non-invasive tool for the early diagnosis and monitoring of CA. However, the specific application of LV STE-derived mechanical dispersion in ATTR and its potential utility in screening first-degree relatives have not been thoroughly investigated. Further research in this area may provide invaluable insights into the early detection and management of this debilitating disease, which can significantly impact patient outcomes if not diagnosed and treated in a timely manner. Understanding the patterns of cardiac mechanics, particularly mechanical dispersion, in ATTR and its at-risk populations could lead to the development of more effective screening and monitoring strategies, ultimately improving the prognosis for patients affected by this condition.

Methods

Study population and study protocol

This was a prospective study conducted at a tertiary cardiac center from 2020 to 2024, supported by a Pfizer research grant (ID#57165999; ClinicalTrials.gov Identifier: NCT05814380)[10]. The study employed a multimodal and genetic cascade screening approach to evaluate 100 consecutive adults who met the enrolment criteria. The analysis encompassed a comprehensive assessment, including clinical data, biochemical tests, electrocardiograms (ECG), echocardiography (TTE), and imaging modalities such as planar whole-body bone scintigraphy and single-photon emission computed tomography/computed tomography (SPECT/CT) with Technetium 99 m and DPD tracer ([^{99m}Tc]Tc-DPD). The diagnosis of ATTR CA was established in accordance with current guidelines, which required the presence of grade 2 or 3 Tc-DPD uptake on planar whole-body scintigraphy, in the absence of monoclonal proteins in the blood and urine[11,12]. In selected cases, where the non-invasive algorithm provided equivocal results, a cardiac or soft tissue biopsy was performed to confirm the final diagnosis[11]. Genetic testing using an amplicon-based next-generation *TTR* sequencing approach was also conducted, and patients with positive free light chain blood immunoglobulins or urine immunofixation were referred to a haematology specialist for a bone marrow biopsy. The inclusion criteria required participants to be over 18 years of age, provide written informed consent, and be diagnosed with ATTR or be a first-degree relative of a patient with ATTR. Exclusion criteria included pregnancy or any other previously diagnosed pre-existing infiltrative disorders. The study cohort was categorised into four groups: Group 1 A comprised patients with variant transthyretin cardiac amyloidosis (ATTRv CA), Group 1B comprised patients with wild-type transthyretin cardiac amyloidosis (ATTRwt CA), Group 2 included asymptomatic carriers of *TTR* pathogenic variants who showed no radiotracer uptake on [^{99m}Tc]Tc-DPD SPECT/CT, and Group 3 consisted of participants without ATTR CA based on genetic testing and [^{99m}Tc]Tc-DPD SPECT/CT findings.

Echocardiography

Echocardiographic examinations were conducted using a Philips EPIQ7 device (The Netherlands) by experienced and blinded operators, consistent with prevailing guidelines[13]. The assessment included standard views for planar measurements, M-mode, and Doppler modalities such as continuous, pulsed, tissue, and colour Doppler. Longitudinal LV strain curves were manually derived from the apical 2-, 3-, and 4-chamber views. The global LV longitudinal strain (GLS), calculated from the peak negative instantaneous average across 18 longitudinal segmental strains, was also evaluated[6,14,15]. Longitudinal strain by speckle-tracking echocardiography was obtained from three standard apical views at a frame rate of approximately 50 frames per second. Strain analysis was performed by averaging five consecutive sinus beats. All echocardiographic acquisitions were ECG-gated. Aortic valve closure (AVC) was determined from pulsed-wave Doppler recordings in the LV outflow tract, synchronised with ECG, and the R–AVC interval was calculated. After identifying the appropriate cardiac cycle, endocardial borders were traced at the end-systolic frame, and an automated tracking algorithm delineated the myocardium in successive frames throughout the cardiac cycle. Tracking quality was verified for each segment, with manual adjustment of the region of interest when necessary. The LV was automatically divided into six segments per view, and global longitudinal strain values were calculated as the average of all segmental values. Mechanical dispersion was derived from the same tracking procedure. Analyses were performed using Philips EPIQ7. Specifically, we conducted a comprehensive assessment of the following parameters across 18 LV segments:

1. Peak systolic longitudinal strain (S) (%): change of myocardial length in the baso-apical direction compared with the initial value;
2. Peak longitudinal strain in cardiac cycle (pS) (%);
3. Time to peak longitudinal strain (TP) (ms): time from R-wave (ECG) to pS;
4. Peak positive strain in early systole (P);
5. LV mechanical dispersion was defined as the standard deviation (SD) of the TP across 18 myocardial segments.

Mechanical dispersion was calculated as the standard deviation of time-to-peak longitudinal strain across the entire cardiac cycle, in accordance with previously published methodology[16]. Analyses were restricted to beats in sinus rhythm, excluding ectopic or paced complexes. To account for cycle length dependency, supplementary analyses were also performed after normalising time-to-peak values to the RR interval and expressing it as a percentage of the cardiac cycle. In addition, sensitivity analyses were performed in the subgroup of patients without bundle-branch block or PR prolongation. An analysis was also performed by restricting peak strain measurements to the systolic phase.

Ground glass appearance of the myocardium was defined as the visual echocardiographic characteristic with a diffuse, increased echogenicity[1]. The apical sparing pattern was defined by a ratio of the average longitudinal strain of the apical segments to that of the basal and mid segments above a 1.0 threshold, moreover '5-5-5' sign was defined according to the published standards as the tissue velocities {'s' [systolic], e' [early diastolic], and a' [late (atrial) diastolic]} measured in Tissue Doppler Imaging (TDI) were all below 5 cm/s[1].

[^{99m}Tc]Tc-DPD SPECT/CT

The [^{99m}Tc]Tc-DPD SPECT/CT imaging procedure and data acquisition adhered to the current recommendations[1,17,18]. Specifically, Technetium 99 m (370–740 MBq) and DPD tracer (TECEOS, CIS BIO) were administered, and planar whole-body bone scans were obtained 2–3 h post-injection. These planar scintigraphic images were evaluated using the Perugini semi-quantitative grading scale (grade 1, 2, or 3)[1,18,19]. Additionally, the CT attenuation-corrected and non-corrected SPECT images were assessed in the coronal, transaxial, and sagittal planes, as well as in three-dimensional maximal-intensity projection cine mode by three experienced nuclear medicine specialists who were blinded to the final diagnosis.

Statistical analysis

For quantitative variables, analysis of variance was employed if the assumptions of homogeneity of variance and normality of residuals were satisfied. In cases where these assumptions were not met, a Box-Cox transformation was applied, and the assumptions were re-evaluated. If the transformed data met the assumptions, ANOVA was conducted on the transformed variables, Tukey's post hoc test was used, which controls the overall family-wise error rate. When the assumptions were still not fulfilled, the non-parametric Kruskal-Wallis ANOVA was utilized with Bonferroni correction. Qualitative variables were analysed using the chi-square test of independence, and pairwise comparisons were performed with Bonferroni correction for multiple testing when a dependency was found. Thus, in all cases, multiple testing was accounted for. Pearson's linear regression was used. In some cases, the use of linear regression and Pearson correlation is doubtful due to the type of data or non-fulfilment of the normality of residuals assumption. In such cases, Spearman's correlation, which is a correlation for the ranks of observations, was applied. Stepwise regression models were then performed. A p-value less than 0.05 was considered statistically significant.

Multivariable modelling was performed in a structured stepwise manner. Univariable models with predictors significant at $p < 0.05$ were first identified. All possible two-variable models were then constructed, retaining only those with both predictors significant. The optimal two-variable model was selected according to the Akaike Information Criterion (AIC). Independence between the final predictors was tested with chi-square. Model stability was assessed using 10,000 bootstrap resamples, with p-value distributions inspected and confidence intervals (CI) reported.

Receiver operating characteristic (ROC) analyses were performed to evaluate the ability of mechanical dispersion, alone and in combination with GLS, to discriminate ATTR CA from controls. The optimal cut-off points were determined using the Youden index. A bivariate logistic regression model was constructed for mechanical dispersion and GLS, and the estimated probability of ATTR CA was derived from model coefficients. Multivariable logistic regression models were constructed including sex, chronic kidney disease (CKD), age, mechanical dispersion, and GLS.

The study prospectively followed patients for 5 years, evaluating the primary end point of all-cause mortality. The survival analyses were performed using Kaplan–Meier estimates and Cox proportional hazards regression models to assess predictors of all-cause mortality. The statistical analyses were carried out using Statistica 13.0 and MedCalc software.

Ethical standards

The study obtained written informed consent from all enrolled participants. All imaging procedures and data acquisition adhered to the current recommendations[1,13,17,18]. The experimental protocol was approved by an Ethics Committee, namely Bioethics Commission at the District Medical Chamber in Kraków, Poland. All procedures were carried out in accordance with the ethical guidelines established by the local Ethics Committee (103/KBL/OIL/2020), the 1964 Helsinki Declaration, and any subsequent revisions, or equivalent ethical standards. The data underlying this study will be made available upon reasonable request to the corresponding author.

Results

The study cohort comprised 100 consecutive participants enrolled between 2020 and 2024, including 27 index patients and 73 asymptomatic first-degree relatives. As summarised in Table 1. The prevalence of *TTR* variants differed significantly among the groups, with 100% of patients in Group 1 A harbouring a *TTR* variant (14 Phe53Leu, 1 Glu109Lys, 1 Glu122Lys, 1 Glu82Lys) and 100% of ATTRv carriers without ATTR CA in Group 2 (14 Phe53Leu, 1 Glu122Lys), while none of the genotype and phenotype negative relatives exhibited a *TTR* variant in Group 3, as well as patients witch ATTRwt CA in Group 1B. Groups 1 A and 1B had a predominance of male participants, and a significantly higher mean age compared to the Group 3 ($p < 0.001$). Additionally, CKD, coronary artery disease was more prevalent in the Groups 1 A and 1B ($p < 0.001$ for all). Patients with ATTR-related CA exhibited higher New York Heart Association (NYHA) functional class, as well as elevated levels of high-sensitivity troponin and N-terminal pro-brain natriuretic peptide (NT-proBNP), relative to the other groups ($p < 0.001$).

Variable	Group 1 A * (*n* = 17)	Group 1B * (*n* = 16)	Group 2 * (*n* = 15)	Group 3 * (*n* = 52)	*p* value
Female gender	**3 (18%)**	**4 (25%)**	9 (60%)	**36 (69%)**	**< 0.001**
Body mass index (kg/m2)	26.7 ± 4.7	27.1 ± 4.3	24.5 ± 4.5	24.6 ± 4.5	0.29
Age (years)	**60.1 ± 7.2**	**75.4 ± 10.6**	**41.3 ± 13.6**	**45.5 ± 12.0**	**< 0.001**
Amyloidosis type					**< 0.001**
-ATTRv	**– 17 (100%)**	**-0 (0%)**	**– 15 (100%)**	**-0 (0%)**	
-ATTRwt	**-0 (0%)**	**-16 (100%)**	**-0 (0%)**	**-0 (0%)**	
Transthyretin variants present	**17 (100%)**	**0 (0%)**	**15 (100%)**	**0 (0%)**	**< 0.001**
CKD	**5 (29%)**	**10 (63%)**	**0 (0%)**	**1 (2%)**	**< 0.001**
Bicep tendon rupture	1 (6%)	1 (6%)	1 (7%)	0 (0%)	0.35
Coronary artery disease	**7 (41%)**	**12 (75%)**	**0 (0%)**	**0 (0%)**	**< 0.001**
NYHA III-IV class	**4 (24%)**	**10 (63%)**	**0 (0%)**	**0 (0%)**	**< 0.001**
Systolic blood pressure (mmHg)	117.4 ± 19.1	111.6 ± 15.1	116.5 ± 16.5	128.3 ± 20.0	**0.007**
Pulmonary congestion	2 (12%)	**5 (31%)**	0 (0%)	**0 (0%)**	**< 0.001**
Haematocrit (%)	40.4 ± 3.8	41.2 ± 5.1	40.8 ± 4.6	41.0 ± 4.1	0.96
Creatinine (mg/dl)	**99.5 ± 41.2**	**111.0 ± 37.5**	**66.5 ± 14.7**	**68.8 ± 14.5**	**< 0.001**
Aspartate transaminase (U/L)	**56.9 ± 123.4**	25.3 ± 8.3	**19.8 ± 5.0**	23.8 ± 9.4	**0.01**
Bilirubin (µmol/L)	**22.5 ± 2.4**	**18.3 ± 13.6**	9.2 ± 4.6	**10.6 ± 10.8**	**0.001**
Gamma-glutamyl transferase (U/L)	**102.7 ± 33.3**	**75.1 ± 37.5**	**24.6 ± 17.9**	**29.2 ± 26.2**	**< 0.001**
NT-proBNP (pg/mL)	**1581.0 [214.0-3165.0]**	**5263.5 [2267.5–8479.0]**	**50.5 [23.0–74.0]**	**56.0 [34.0–80.0]**	**< 0.001**
Cardiac troponin T (ng/mL)	**0.038 [0.020–0.086]**	**0.058 [0.042–0.094]**	**0.003 [0.003–0.004]**	**0.004 [0.003–0.005]**	**< 0.001**
Albumin (g/L)	56.7 ± 23.8	36.8 ± 3.9	39.3 ± 2.7	39.3 ± 3.1	0.07
Electrocardiogram - low voltage	**10 (59%)**	**7 (44%)**	3 (20%)	**3 (6%)**	**< 0.001**
Electrocardiogram - q	**4 (24%)**	1 (6%)	0 (0%)	**1 (2%)**	**0.003**
Electrocardiogram - ST-T abnormalities	**9 (53%)**	4 (25%)	2 (13%)	**5 (10%)**	**< 0.001**
Atrioventricular block	**5 (29%)**	**10 (63%)**	**0 (0%)**	**0 (0%)**	**< 0.001**
Perugini grade					
– 0	**0 (0%)**	**0 (0%)**	**15 (100%)**	**52 (100%)**	**< 0.001**
– 1	**1 (6%)**	**0 (0%)**	**0 (0%)**	**0 (0%)**	
– 2	**3 (18%)**	**3 (19%)**	**0 (0%)**	**0 (0%)**	
– 3	**13 (76%)**	**13 (81%)**	**0 (0%)**	**0 (0%)**	

Table 1. Clinical characteristics of the study population.*Categorical data are presented as percentage, while continuous variables are reported as the mean ± one standard deviation or the median (IQR). Values considered statistically significant are indicated in bold font. ATTRwt - transthyretin amyloidosis wild-type; ATTRv - hereditary transthyretin amyloidosis; CKD - chronic kidney disease; NYHA - New York Heart Association class; NT-proBNP - N-terminal pro-brain natriuretic peptide.

Echocardiographic assessment revealed that Groups 1A and 1B displayed greater LV wall thickness, LV mass index, left atrial area and volume, alongside reduced LV ejection fraction (LVEF), more advanced diastolic dysfunction, and an 'apical sparing' pattern, compared to the other groups ($p < 0.001$) (Table 2). Additionally, participants in Groups 1A and 1B exhibited significantly elevated right ventricle (RV) wall thickness, larger right atrial area and volume, reduced RV systolic function (TDI RV S', tricuspid annular plane systolic excursion (TAPSE), and RV outflow tract velocity time integral (VTI)), compared to the other study groups ($p < 0.05$ for all). The echocardiographic evaluation of LV longitudinal strain parameters revealed significant differences across groups in multiple parameters. Specifically, compared to Groups 2 and 3, Group 1 A and 1B exhibited significantly reduced GLS, and segmental longitudinal strain across the apical 2-, 3-chamber views ($p < 0.001$ for all). Significant differences were also observed in basal, mid, and apical segments, with Group 1B consistently showing lower strain values in most segments. This heterogeneous pattern of reduced strain, with more pronounced impairment in certain regions compared to others, likely reflects the patchy distribution of amyloid infiltration within the myocardium in ATTR CA, resulting in 'apical sparing' pattern. Furthermore, Groups 1 A and 1B exhibited significantly greater mechanical dispersion compared to Groups 2 and 3 (Fig. 1).

The study further investigated the relationships between mechanical dispersion and various clinical characteristics (Table 3, Fig. 2). Mechanical dispersion exhibited positive correlations with age, NYHA class, LV mass index, E/E' ratio, RV wall thickness, and levels of NT-proBNP and Perugini grade ($p < 0.05$ for all). Conversely, it correlated negatively with LVEF, GLS, and six-minute walk test results ($p < 0.05$ for all). Additionally, patients with ATTRwt demonstrated significantly greater mechanical dispersion compared to

Variable	Group 1 A * (*n* = 17)	Group 1B * (*n* = 16)	Group 2 * (*n* = 15)	Group 3 * (*n* = 52)	*p* value
R-AVC (ms)	322.6 ± 58.5	327.2 ± 98.9	361.3 ± 56.1	351.2 ± 48.7	0.04
GLS (%)	**– 15.1 ± 5.4**	**– 10.8 ± 4.1**	**– 19.4 ± 3.5**	**– 19.2 ± 3.6**	**< 0.001**
LV mechanical dispersion calculated as the standard deviation of time-to-peak longitudinal strain across the entire cardiac cycle (ms)	**85.1 ± 20.9**	**109.3 ± 21.1**	**71.8 ± 17.9**	**72.2 ± 22.3**	**< 0.001**
LV mechanical dispersion normalised to heart rate [%]	9.7 ± 2.2	**11.9 ± 2.6**	**8.1 ± 2.2**	**8.1 ± 2.2**	**< 0.001**
LV mechanical dispersion restricted to patients without conduction abnormalities	85.0 ± 25.1	98.200 ± 9.4	71.8 ± 17.9	71.9 ± 22.2	**0.02**
LV mechanical dispersion restricted to systole	29.9 ± 27.0	29.7 ± 19.3	29.9 ± 24.5	27.9 ± 18.1	0.97
S-apical 2-chamber view (%)	**– 15.2 ± 6.9**	**– 10.0 ± 5.3**	**– 18.0 ± 4.2**	**– 20.1 ± 4.2**	**< 0.001**
S-apical 3-chamber view (%)	**– 13.9 ± 5.4**	**– 7.9 ± 4.9**	**– 21.7 ± 5.2**	**– 18.9 ± 4.2**	**< 0.001**
S-apical 4-chamber view (%)	– 15.7 ± 6.1	**– 10.5 ± 5.9**	**– 18.2 ± 5.6**	**– 19.1 ± 3.6**	**< 0.001**
S basal anteroseptal (%)	**– 9.9 ± 4.5**	**– 8.7 ± 3.6**	**– 17.9 ± 6.8**	**– 17.1 ± 8.5**	**< 0.001**
S mid anteroseptal (%)	**– 14.9 ± 7.3**	**– 6.5 ± 6.2**	**– 20.2 ± 7.9**	**– 20.0 ± 7.6**	**< 0.001**
S apical anteroseptal (%)	– 19.9 ± 9.8	– 18.0 ± 8.1	– 23.7 ± 10.8	– 20.8 ± 7.9	0.36
S basal anterior (%)	**– 11.2 ± 8.5**	**– 5.6 ± 5.1**	**– 19.3 ± 11.1**	**– 20.2 ± 9.7**	**< 0.001**
S mid anterior (%)	– 14.9 ± 7.9	– 12.8 ± 5.4	– 15.2 ± 8.1	– 18.5 ± 7.4	0.03
S apical anterior (%)	– 20.8 ± 8.7	– 16.6 ± 7.9	– 16.2 ± 7.3	– 17.4 ± 7.7	0.33
S basal anterolateral (%)	**– 11.2 ± 9.8**	**– 5.6 ± 3.5**	**– 24.2 ± 11.4**	**– 21.7 ± 9.6**	**< 0.001**
S mid anterolateral (%)	– 12.5 ± 8.7	– 13.7 ± 7.5	– 14.8 ± 6.4	– 16.7 ± 5.8	0.11
S apical anterolateral (%)	– 24.5 ± 7.4	– 18.7 ± 10.0	– 17.9 ± 6.7	– 18.2 ± 6.8	0.03
S basal inferolateral (%)	**– 10.3 ± 9.8**	**– 6.1 ± 5.9**	**– 26.7 ± 11.6**	**– 21.7 ± 9.9**	**< 0.001**
S mid inferolateral (%)	– 13.0 ± 7.6	– 11.7 ± 5.5	– 13.6 ± 6.5	– 16.2 ± 8.1	0.12
S apical inferolateral (%)	– 20.3 ± 8.8	– 16.9 ± 8.8	– 22.8 ± 7.9	– 20.4 ± 7.0	0.22
S basal inferior (%)	**– 10.4 ± 8.9**	**– 5.0 ± 6.1**	**– 13.8 ± 7.4**	**– 19.3 ± 8.8**	**< 0.001**
S mid inferior (%)	**– 14.1 ± 7.2**	**– 10.7 ± 4.7**	**– 20.9 ± 6.2**	**– 20.8 ± 6.5**	**< 0.001**
S apical inferior (%)	– 20.9 ± 7.9	**– 16.5 ± 8.7**	– 20.5 ± 7.2	**– 24.1 ± 7.4**	**0.008**
S basal inferoseptal (%)	– 10.8 ± 7.6	**– 6.4 ± 5.3**	**– 12.5 ± 6.4**	**– 14.2 ± 6.1**	**0.006**
S mid inferoseptal (%)	**– 13.9 ± 6.6**	**– 10.1 ± 3.9**	**– 19.6 ± 6.9**	**– 20.3 ± 4.4**	**< 0.001**
S apical inferoseptal (%)	– 19.8 ± 8.7	– 19.9 ± 8.9	– 25.5 ± 6.9	– 24.7 ± 4.9	0.08
LV interventricular septum thickness (mm)	**17.9 ± 3.8**	**20.8 ± 1.9**	**10.2 ± 1.7**	**11.1 ± 2.3**	**< 0.001**
LV posterior wall thickness (mm)	**17.3 ± 3.8**	**18.8 ± 4.1**	**9.8 ± 1.9**	**10.6 ± 2.1**	**< 0.001**
LV maximum wall thickness (mm)	**18.8 ± 4.5**	**22.3 ± 1.9**	**10.5 ± 1.7**	**11.7 ± 2.2**	**< 0.001**
LV mass index (g/m2)	**203.6 ± 79.2**	**213.7 ± 30.5**	**84.9 ± 21.7**	**96.3 ± 26.5**	**< 0.001**
LV end-diastolic diameter (mm)	46.1 ± 7.4	41,3 ± 6.1	45.1 ± 4.8	45.4 ± 5.7	0.09
LV end-diastolic volume (ml)	**115.6 ± 41.5**	**82.9 ± 36.9**	101.4 ± 19.8	96.1 ± 27.0	**0.04**
Left atrium area (cm^2)	**26.6 ± 5.8**	**32.5 ± 6.7**	**17.6 ± 4.2**	**17.2 ± 3.9**	**< 0.001**
Left atrium volume index (ml/m^2)	**46.3 ± 13.9**	**62.4 ± 21.5**	**26.6 ± 9.0**	**25.7 ± 9.4**	**< 0.001**
LV ejection fraction (%)	**47.8 ± 14.5**	**38.3 ± 9.6**	**61.6 ± 4.0**	**62.3 ± 4.9**	**< 0.001**
Stroke volume (ml)	65.5 ± 23.1	48.4 ± 15.1	67.1 ± 0.7	61.7 ± 20.5	0.06
LV VTI (cm)	20.5 ± 7.7	**16.2 ± 4.3**	**22.4 ± 4.2**	**21.7 ± 4.8**	**0.004**
E/A	**1.4 ± 0.7**	**2.4 ± 0.8**	**1.4 ± 0.4**	**1.2 ± 0.4**	**0.001**
E/E'	**18.3 ± 11.2**	**21.2 ± 8.9**	**6.1 ± 1.9**	**7.3 ± 1.8**	**< 0.001**
LV lateral wall TDI S'(cm/s)	**5.2 ± 1.8**	**4.5 ± 2.7**	**9.0 ± 2.3**	**8.1 ± 2.5**	**< 0.001**
LV lateral wall TDI E' (cm/s)	**7.4 ± 2.8**	**6.0 ± 2.5**	**15.2 ± 3.5**	**13.7 ± 4.5**	**< 0.001**
LV lateral wall TDI A' (cm/s)	**7.2 ± 4.1**	**3.7 ± 1.8**	**9.4 ± 2.6**	**9.9 ± 2.9**	**< 0.001**
LV interventricular septum TDI S' (cm/s)	**4.7 ± 1.5**	**4.1 ± 1.3**	**7.2 ± 1.2**	**7.3 ± 1.6**	**< 0.001**
LV interventricular septum TDI E' (cm/s)	**8.6 ± 5.1**	**3.9 ± 1.5**	**10.2 ± 2.0**	**10.7 ± 7.9**	**< 0.001**
LV interventricular septum TDI A' (cm/s)	**6.9 ± 3.8**	**3.2 ± 2.2**	**8.2 ± 2.1**	**8.6 ± 2.6**	**< 0.001**
RV thickness (mm)	**7.3 ± 2.9**	**6.9 ± 1.7**	**4.3 ± 1.1**	**4.7 ± 1.9**	**< 0.001**
RV outflow tract diameter (mm)	**34.0 ± 7.7**	**34.0 ± 5.8**	**28.6 ± 5.0**	**27.9 ± 4.7**	**< 0.001**
Right atrium area (cm^2)	**24.1 ± 6.7**	**27.7 ± 8.2**	**15.0 ± 3.5**	**14.6 ± 3.9**	**< 0.001**
Right atrium volume index (ml/m^2)	**14.7 ± 13.9**	**53.4 ± 17.9**	**19.8 ± 5.7**	**20.3 ± 6.6**	**< 0.001**
RV VTI (cm)	**16.7 ± 6.0**	**11.6 ± 2.7**	**16.3 ± 3.4**	**17.6 ± 3.8**	**< 0.001**
TAPSE (mm)	**17.4 ± 4.9**	**13.7 ± 5.5**	**23.9 ± 3.5**	**22.8 ± 3.2**	**< 0.001**
sPAP (mmHg)	**31.2 ± 13.5**	**35.9 ± 9.8**	**21.4 ± 5.8**	**22.0 ± 5.0**	**< 0.001**
RV TDI S' (cm/s)	**9.2 ± 3.0**	**7.9 ± 3.1**	**12.3 ± 2.1**	**12.5 ± 2.3**	**< 0.001**
RV TDI E' (cm/s)	**8.1 ± 2.4**	**8.3 ± 4.1**	**11.7 ± 4.4**	**12.9 ± 3.6**	**< 0.001**
Continued					

Variable	Group 1 A * (*n* = 17)	Group 1B * (*n* = 16)	Group 2 * (*n* = 15)	Group 3 * (*n* = 52)	*p* value
RV TDI A'(cm/s)	**9.8 ± 6.2**	**6.4 ± 4.6**	**13.8 ± 5.7**	**13.3 ± 3.9**	**< 0.001**
Apical sparing	**11 (65%)**	**14 (88%)**	**3 (20%)**	**16 (31%)**	**< 0.001**
Ground glass appearance of myocardium	16 (94%)	15 (94%)	13 (87%)	38 (73%)	**0.04**
"5-5-5" sign	**4 (24%)**	**8 (50%)**	**0 (0%)**	**0 (0%)**	**< 0.001**

Table 2. Echocardiographic assessment within the groups. * Categorical data are presented as percentage, while continuous variables are reported as the mean ± one standard deviation or the median (IQR). Values considered statistically significant are indicated in bold font. Abbreviations are listed in the Table 1 legend. GLS - global longitudinal strain; LV - left ventricle; RV - right ventricle; S - peak systolic longitudinal strain; sPAP - systolic pulmonary artery pressure; TAPSE - tricuspid annular plane systolic excursion; TDI - Tissue Doppler Imaging; VTI -Velocity Time Integral.

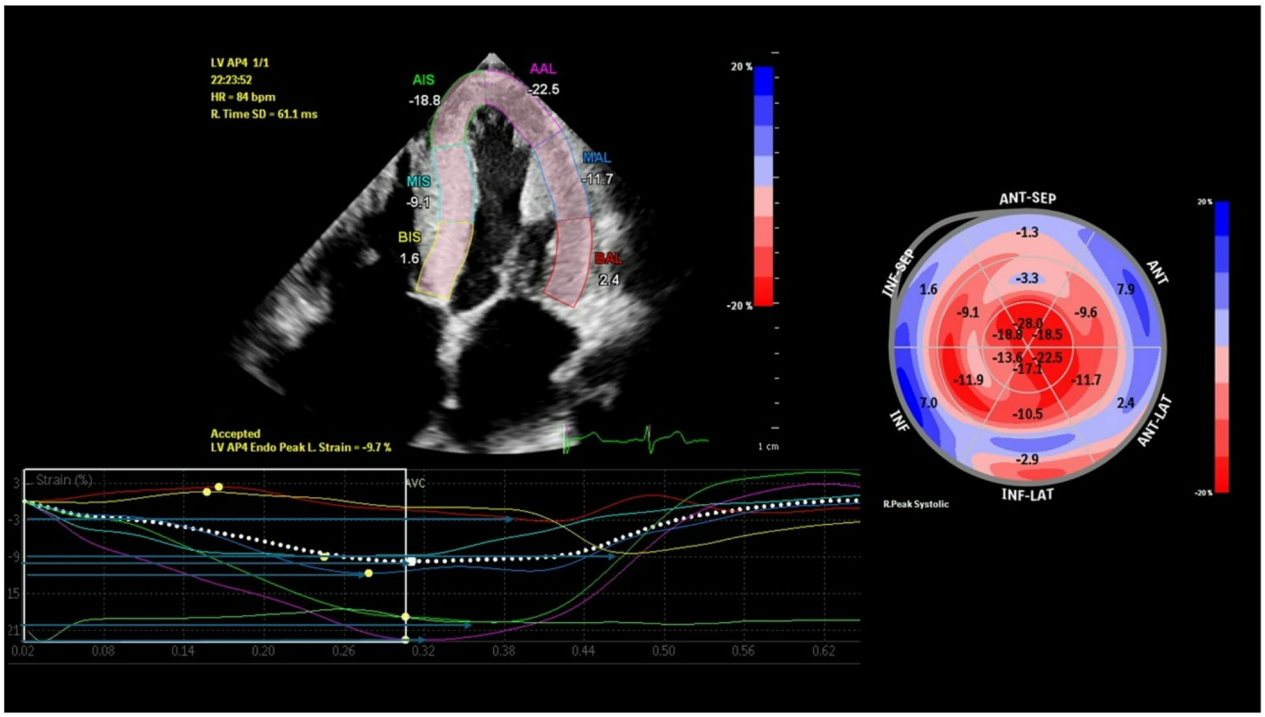

Fig. 1. Imaging results in a patient with hereditary transthyretin amyloidosis in apical 4-chamber view are consistent with advanced cardiac involvement and increased value of LV mechanical dispersion to 92 [ms], which was defined as the standard deviation of the time from QRS peak in electrocardiogram to peak longitudinal strain across the entire cardiac cycle. Horizontal blue arrows indicate contraction durations in each segment.

those with hereditary ATTR (ATTRv) ($p < 0.05$ for all). Moreover, male gender, carpal tunnel syndrome, apical sparing, '5-5-5' sign was associated with increased mechanical dispersion ($p < 0.05$ for all). The multivariable stepwise regression model revealed that the variables best describing mechanical dispersion selected on the basis of AIC were ATTRwt and the '5-5-5' sign ($p = 0.012$ and $p = 0.002$, respectively). The chi-square test indicated no significant dependence between the two predictors ($p = 0.073$). Bootstrap resampling ($n = 10{,}000$) confirmed the stability of the model: the 95% confidence interval for the p-values ranged from 0.000 to 0.086 for '5-5-5' sign and from 0.000 to 0.232 for ATTRwt.

ROC analysis showed that mechanical dispersion discriminated ATTR CA from controls with an AUC of [0.789], with an optimal cut-off of 81.3 ms (Youden index) (Fig. 3). A logistic regression model incorporating both mechanical dispersion and GLS yielded an AUC of [0.833], with the estimated probability of ATTR CA calculated (Fig. 4). The optimal cut-off probability was 0.462 (Table 4). Mechanical dispersion was higher in patients with CKD. A multivariable model including sex, CKD, age, mechanical dispersion, and GLS confirmed that mechanical dispersion remained associated with ATTR CA after adjustment.

Analyses performed with mechanical dispersion normalised to the RR interval yielded results consistent with those obtained using absolute time values, with differences between ATTR CA and control groups remaining highly significant ($p < 0.001$). Associations with disease severity markers also remained significant after

Variable	MD *p* value	MDN *p* value	MDE *p* value	MDS *p* value
ATTRwt	**0.003**	**< 0.001**	**0.02**	0.97
Male gender	**0.002**	**0.003**	**0.009**	0.62
Age	**< 0.001**	**< 0.001**	**< 0.001**	0.23
Carpal tunnel syndrome	**0.004**	0.059	0.12	**0.04**
NYHA	**< 0.001**	**< 0.001**	**0.03**	0.42
NT-proBNP	**< 0.001**	**< 0.001**	**< 0.001**	0.23
Perugini grade	**< 0.001**	**< 0.001**	**0.002**	0.051
Six-minute walk test	**< 0.001**	**< 0.001**	**< 0.001**	0.21
LV mass index	**< 0.001**	**< 0.001**	**< 0.001**	0.20
LV ejection fraction	**< 0.001**	**< 0.001**	**0.01**	0.16
GLS	**< 0.001**	**< 0.001**	**0.001**	0.62
Apical sparing	**0.01**	**0.02**	**0.03**	0.78
E/E'	**< 0.001**	**< 0.001**	**< 0.001**	0.08
RV wall thickness	**0.003**	**0.006**	**0.049**	0.69
TAPSE	**< 0.001**	**< 0.001**	**0.017**	0.52
RV VTI	**0.001**	**0.002**	0.07	0.86
RV TDI S'	**< 0.001**	**< 0.001**	**0.03**	0.49
''5-5-5" sign	**0.001**	**< 0.001**	**0.006**	0.28

Table 3. The associations of LV mechanical dispersion calculated as the standard deviation of time-to-peak longitudinal strain across the entire cardiac cycle (MD), normalised time-to-peak values to the RR interval and expressing it as a percentage of the cardiac cycle (MDN), restricted to patients without conduction abnormalities (MDE) and restricted to systole (MDS). * Values considered statistically significant are indicated in bold font. Abbreviations are listed in the legends of Tables 1 and 2.

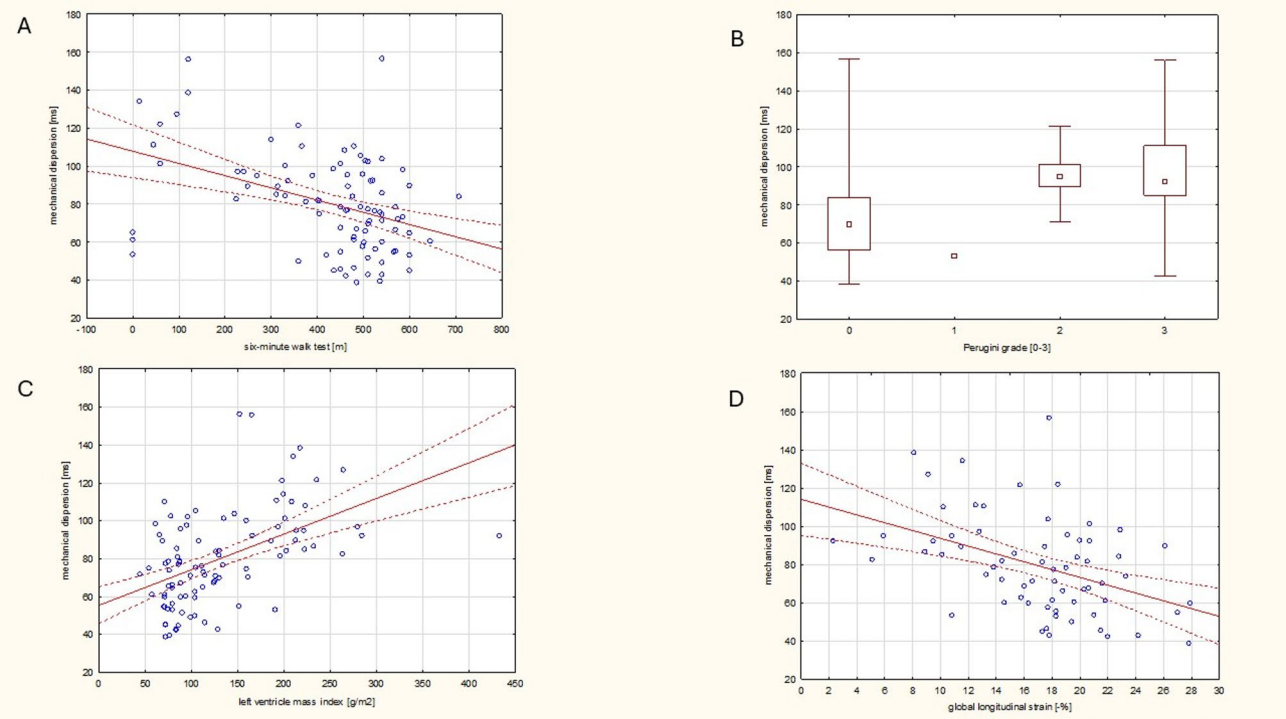

Fig. 2. The correlations of LV mechanical dispersion value [ms] calculated as the standard deviation of time-to-peak longitudinal strain across the entire cardiac cycle with the six-minute walk test results [m] (panel (**A**), $p < 0.001$, $r = -0.41$), Perugini grades (panel (**B**), $p < 0.001$, $\rho = 0.475$), LV mass index [g/m^2] (panel (**C**), $p < 0.001$, $r = 0.50$), and global longitudinal strain value [%] (panel (**D**), $p < 0.001$, $r = -0.43$). Correlation analyses were performed, with Pearson's correlation coefficient (r) for Panels (**A**), (**C**), and (**D**), and Spearman's rank correlation coefficient (ρ) for Panel (**B**).

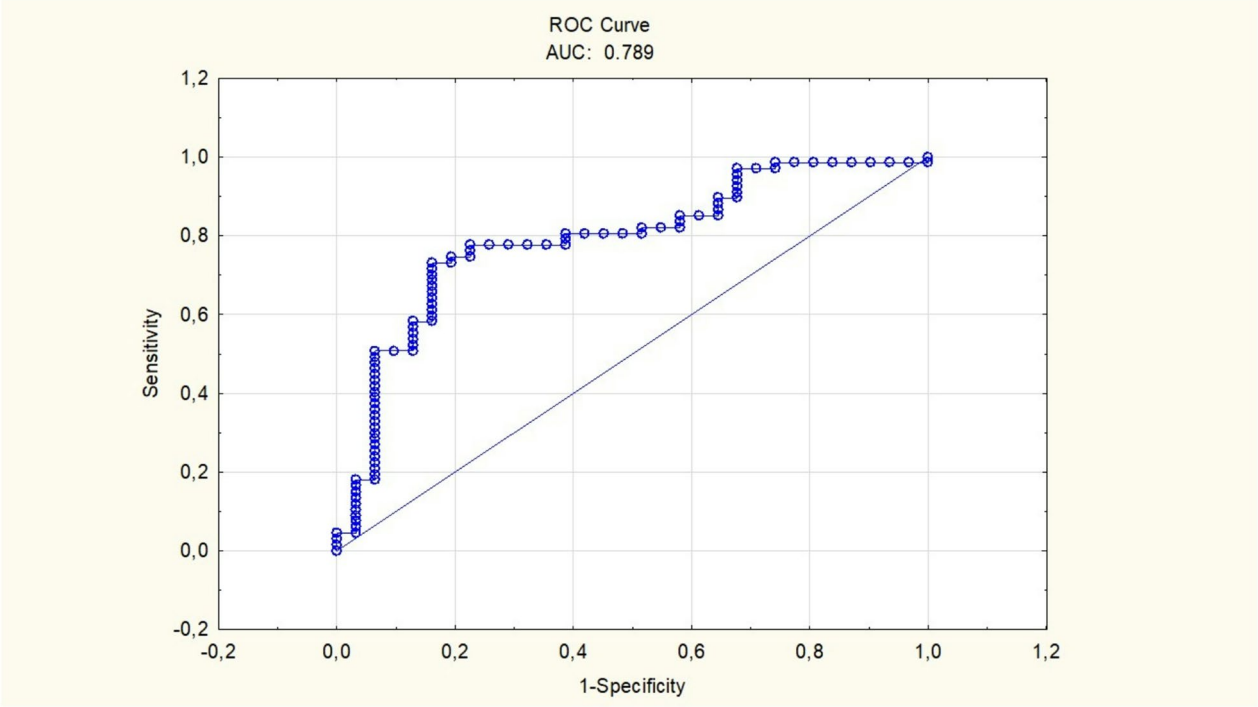

Fig. 3. Receiver operating characteristic (ROC) curve for mechanical dispersion in discriminating transthyretin cardiac amyloidosis from controls.

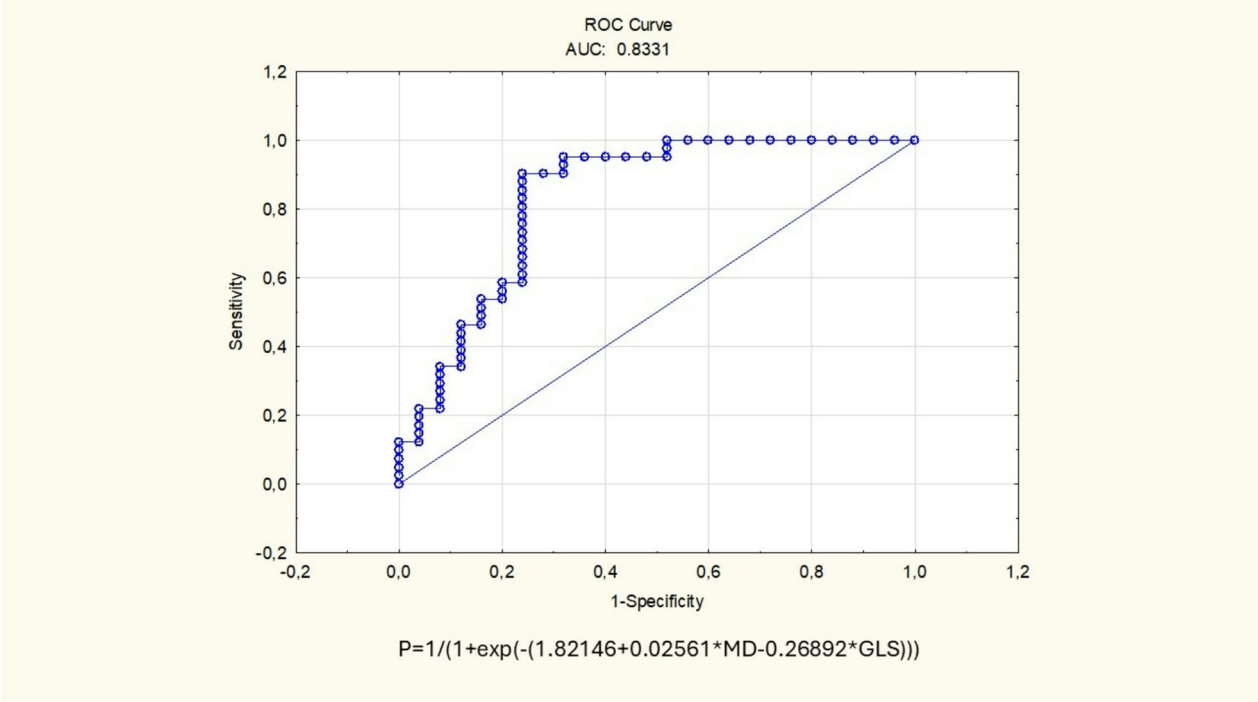

Fig. 4. Receiver operating characteristic (ROC) curve for the combined logistic regression model of mechanical dispersion (MD) and global longitudinal strain (GLS) in discriminating transthyretin cardiac amyloidosis from controls.

Variable	HR	95% CI lower bound	95% CI upper bound	*p* value
LV mechanical dispersion calculated as the standard deviation of time-to-peak longitudinal strain across the entire cardiac cycle	**1.03**	**1.01**	**1.06**	**0.004**
LV mechanical dispersion restricted to systole	0.98	0.95\	1.02	0.52
LV mechanical dispersion normalised to heart rate	**1.43**	**1.14**	**1.81**	**0.002**
Age	**1.06**	**1.02**	**1.09**	**0.002**
GLS	**0.87**	**0.78**	**0.97**	**0.008**
Conduction abnormalities	**3.61**	**1.09**	**11.89**	**0.03**
Female gender	0.31	0.08	1.19	0.09
Coronary artery disease	13.86	3.67	52.48	**< 0.001**
CKD	0.03	0.01	572.91	0.48

Table 4. Univariable Cox regression analysis was performed to examine the associations of all-cause mortality. * Abbreviations are listed in the Tables 1, and 2 legends. Unadjusted analyses with hazard ratios (HR) and 95% CI.

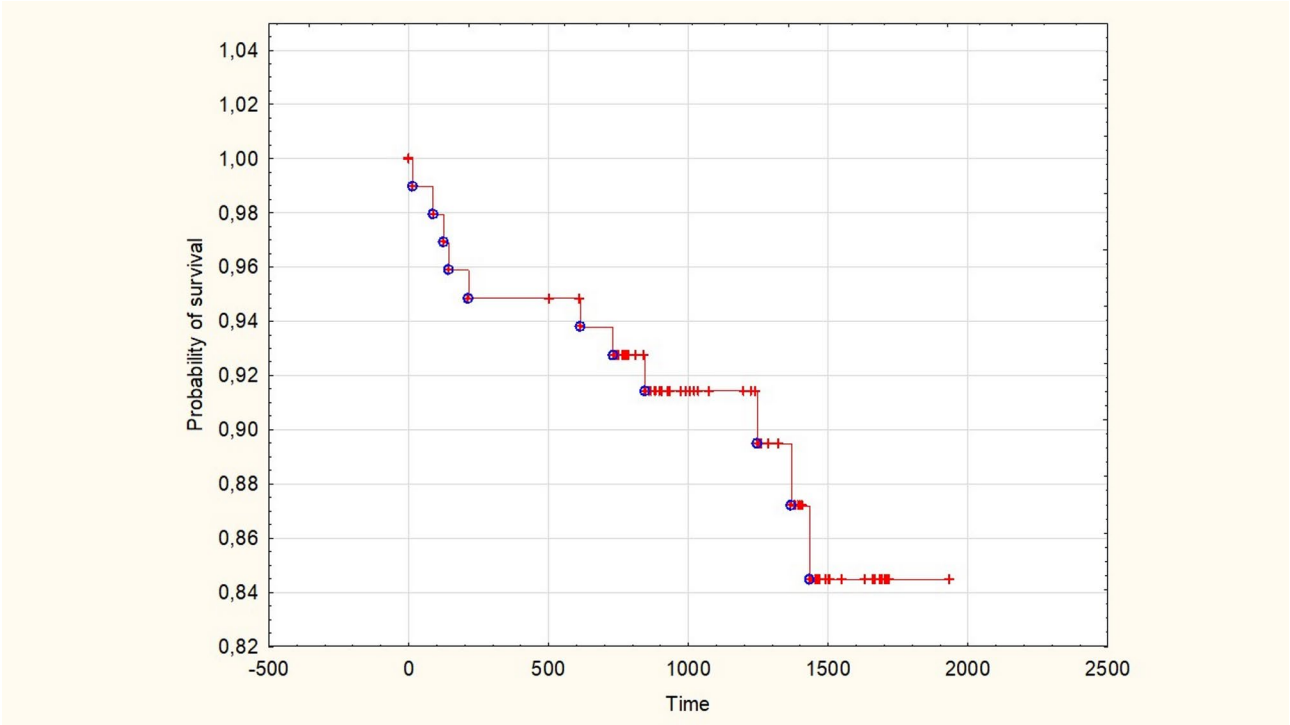

Fig. 5. Shows the results of the analysis of all-cause mortality rates with the use of the Kaplan-Meier method.

correction for heart rate. All group differences and correlations with clinical variables were unchanged, except that the previously observed significant association with carpal tunnel syndrome was lost after RR normalisation. Similarly, sensitivity analyses restricted to patients without conduction abnormalities (bundle-branch block or PR prolongation) confirmed that the principal findings were unchanged, including the correlations with ATTR CA status, and clinical as well as imaging parameters, with the exception of carpal tunnel syndrome and RV VTI, where the association did not persist after adjustment for conduction abnormalities.

Further analysis restricting peak strain to systole did not demonstrate significant differences between groups and correlations with clinical data and scintigraphic findings, except for a significant association with carpal tunnel syndrome; notably, patients with carpal tunnel syndrome had lower values ($p = 0.04$). In contrast, full-cycle analysis revealed clinically relevant group differences, consistent with the altered myocardial mechanics characteristic of ATTR CA.

During follow-up, the was a reduced survival in patients with higher mechanical dispersion measured during the entire cardiac cycle and normalised to the heart rate (Fig. 5). In univariable Cox regression, mechanical dispersion (hazard ratio (HR) = 1.03, 95% CI 1.01–1.06, $p = 0.004$), normalised mechanical dispersion (HR = 1.43, 95% CI 1.14–1.81, $p = 0.002$), age (HR = 1.06, 95% CI 1.02–1.10, $p = 0.002$), GLS (HR = 0.87, 95% CI 0.78–0.97, $p = 0.009$), and conduction abnormalities (HR = 3.61, 95% CI 1.10–11.90, $p = 0.035$) were significant predictors of mortality (Table 4). The optimal multivariable model included normalised to heart rate mechanical dispersion

(HR = 1.34, 95% CI 1.02–1.77, $p = 0.035$) and age (HR = 1.05, 95% CI 1.002–1.09, $p = 0.038$), both of which remained independent predictors of outcome.

Discussion

Transthyretin cardiac amyloidosis is a severe, progressive, and often underdiagnosed disease that has undergone significant epidemiological and clinical changes in recent years[2]. Historically, ATTR CA was considered a rare disorder, but increased disease awareness and advancements in diagnostic techniques have led to a better understanding of its true prevalence, which is now reported to be higher globally, particularly among the elderly population[11]. The epidemiological shift has been accompanied by an evolution in the clinical presentation of ATTR CA[18]. The disease can now manifest with a broader spectrum of symptoms, ranging from subtle cardiac impairment to overt heart failure. In some cases, the onset of ATTR CA has become more insidious, posing diagnostic challenges. Furthermore, the potential treatment options for ATTR CA have undergone a significant transformation in recent years[2,11,17]. The emergence of novel targeted therapies, such as TTR stabilisers and *TTR* gene silencers, has brought renewed hope for the management of this previously devastating condition[2]. These advancements have the potential to significantly improve outcomes for patients with ATTR CA, emphasising the importance of early diagnosis and the implementation of personalized care approaches in this complex disease. Early recognition of the disease, coupled with the implementation of tailored treatment strategies, can significantly impact the prognosis and quality of life for patients affected by this progressive and debilitating condition[5].

The cardiac amyloid deposition impacts profoundly the mechanical properties of the myocardium, leading to characteristic echocardiographic findings such as increased LV wall thickness, reduced longitudinal deformation, and impaired relaxation, which are related to heart failure progression[1]. Nuclear imaging techniques such as cardiac scintigraphy with Tc-99 m-labelled bone-seeking tracers (e.g., Perugini grading) have become essential in the diagnosis of ATTR CA, complementing the echocardiographic assessment of the disease[1,12,17–19]. Furthermore, the development of STE has provided additional insights into the functional and mechanical derangements associated with CA[8,13,14]. Our study demonstrates that mechanical dispersion of the LV myocardium is significantly increased in patients with ATTR CA compared to their unaffected first-degree relatives. This finding suggests that increased mechanical dispersion may be a sensitive marker of early cardiac involvement in ATTR. Mechanical dispersion, which reflects the heterogeneity in the timing and magnitude of regional myocardial deformation, has been previously reported as a sensitive marker of cardiac dysfunction in various cardiomyopathies, including hypertrophic, dilated, and restrictive forms[20]. In the context of ATTR CA, the observed increase in mechanical dispersion is likely a consequence of the heterogeneous distribution of amyloid infiltration within the myocardium. This patchy deposition of amyloid can lead to regional differences in myocardial deformation, with some areas exhibiting impaired function while others may maintain relatively preserved contraction[14,21]. Previous studies have reported a similar pattern of regional myocardial dysfunction, where not only the infarct and border zones but also the remote myocardium can exhibit impaired contractile function in the setting of myocardial infarction[22]. This heterogeneous impairment of myocardial deformation has been attributed to various factors, such as interstitial fibrosis, microvascular dysfunction, and electromechanical dyssynchrony. Similarly, in ATTR CA, the patchy distribution of amyloid deposition within the myocardium may contribute to the observed increase in mechanical dispersion. This regional heterogeneity in myocardial deformation can have important implications for the course of the disease in these patients. Increased mechanical strain dispersion has been associated with clinical outcomes in hypertrophic cardiomyopathy, mitral valve prolapse, and ischaemic heart failure[23–27]. Furthermore, LV mechanical dispersion as found to be an independent predictor of adverse events in individuals with aortic stenosis, even after adjusting for established risk factors[28].

In our study increased mechanical dispersion was associated with advanced disease stages, presence of ATTRwt, as well as specific electrocardiographic and echocardiographic features known to be associated with poor prognosis in ATTR CA. These findings suggest that mechanical dispersion may serve as a valuable marker of disease severity and risk stratification in ATTR CA patients. The robustness of findings after normalisation to the RR interval further supports the validity of mechanical dispersion as a disease marker in ATTR CA, independent of heart rate variability. Moreover, additional analyses indicate that the observed differences in mechanical dispersion are attributable to disease-related mechanical heterogeneity rather than conduction abnormalities. Although comorbidities such as CKD were associated with higher mechanical dispersion, the adjusted modelling confirmed that these factors did not account for the observed association between mechanical dispersion and ATTR CA. In supplementary analyses restricting peak strain to the systolic phase, no significant group differences or correlations with clinical variables were observed. By contrast, full-cycle measurements captured disease-related alterations, indicating that this approach provides a more appropriate assessment of LV mechanics in ATTR CA. Prospective follow-up analyses demonstrated that normalised to heart rate mechanical dispersion and mechanical dispersion measured during the entire cardiac cycle were independent predictors of all-cause mortality, suggesting potential prognostic value of mechanical dispersion in ATTR CA.

This study underscores the pivotal role of echocardiography as a vital diagnostic tool in the routine clinical management of patients with ATTR CA. Importantly, specific echocardiographic parameters, such as global longitudinal strain, apical sparing ratio, RV to pulmonary artery coupling index, global and free wall longitudinal RV strain, as well as right and left atrial strain have been shown to have significant prognostic implications in this patient population[1,8,11,14,29,30]. The comprehensive echocardiographic assessment can facilitate diagnosis of ATTR CA, enable close monitoring of the disease progression, and guide the implementation of tailored treatment strategies, ultimately improving the overall management and outcomes for this challenging patient cohort. By providing detailed information about cardiac structure, function, and mechanics, echocardiography plays a crucial role in the evaluation and risk stratification of individuals with ATTR CA. In addition to strain-derived timing dispersion, LV mechanics may also be assessed using hemodynamic forces (HDFs), vectorial

markers based on strain or 4D flow analysis, which reflect intraventricular pressure gradients and synchrony of force generation[31]. This approach may be particularly relevant in amyloidosis, future studies should therefore examine HDF-based metrics in this population.

Limitations

This study has several limitations that should be considered. The sample size was relatively small, which may limit the generalizability of the findings. Additionally, the cross-sectional design of the study precludes the assessment of longitudinal changes in mechanical dispersion over time. Longitudinal evaluations would be valuable to determine how mechanical dispersion evolves as the disease progresses and to further elucidate its potential role in disease monitoring and risk stratification for patients with ATTR CA. Future studies with larger sample sizes and a longitudinal framework would help address these limitations and provide deeper insights into the applications of STE-derived mechanical dispersion in this patient population. Intra- and inter-observer reproducibility of GLS and mechanical dispersion was not formally assessed in this study, which is a limitation; however, previous studies have reported good reproducibility of these indices[16].

Conclusions

In summary, our study demonstrates that LV mechanical dispersion, as assessed by STE, is significantly increased in patients with ATTR CA compared to their unaffected first-degree relatives. This finding may reflect the heterogeneous distribution of amyloid infiltration within the myocardium and could provide insights into the pathophysiology of cardiac involvement in this disease. Furthermore, increased LV mechanical dispersion was associated with advanced disease stage and the presence of ATTRwt, as well as specific clinical and echocardiographic markers of poor prognosis, suggesting that it may serve as a valuable tool for disease assessment and risk stratification in ATTR CA patients. Importantly, mechanical dispersion demonstrates prognostic value, with higher values associated with poorer long-term survival. These findings highlight the potential utility of STE-derived parameters in the comprehensive evaluation of cardiac involvement in ATTR CA and warrant further investigation in larger, longitudinal studies.

Data availability

The data underlying this study will be made available upon reasonable request to the corresponding author.

Received: 14 February 2025; Accepted: 28 October 2025
Published online: 27 November 2025

References

1. Dorbala, S. et al. ASNC/AHA/ASE/EANM/HFSA/ISA/SCMR/SNMMI expert consensus recommendations for multimodality imaging in cardiac amyloidosis: part 1 of 2—evidence base and standardized methods of imaging. *J. Nucl. Cardiol.* **26**, 2065–2123. https://doi.org/10.1007/s12350-019-01760-6 (2019).
2. Arbelo, E. et al. 2023 ESC guidelines for the management of cardiomyopathies. *Eur. Heart J.* **44**, 3503–3626. https://doi.org/10.1093/eurheartj/ehad194 (2023).
3. Holcman, K. et al. Transthyretin amyloid cardiomyopathy in patients with unexplained increased left ventricular wall thickness. *Int. J. Cardiovasc. Imaging*. https://doi.org/10.1007/s10554-024-03158-z (2024).
4. Petkow-Dimitrow, P., Rajtar-Salwa, R., Holcman, K., Kostkiewicz, M. & Rubiś, P. From hypertrophic cardiomyopathy to transthyretin amyloidosis: an unusual case and challenging diagnosis. *Pol. Arch. Intern. Med.* **130**, 153–154. https://doi.org/10.20452/pamw.15140 (2020).
5. Arbustini, E. & Merlini, G. Early identification of transthyretin-related hereditary cardiac amyloidosis. *JACC Cardiovasc. Imaging.* **7**, 511–514. https://doi.org/10.1016/j.jcmg.2014.03.007 (2014).
6. Voigt, J. U. et al. Definitions for a common standard for 2D speckle tracking echocardiography: consensus document of the EACVI/ASE/Industry task force to standardize deformation imaging. *J. Am. Soc. Echocardiogr.* **28**, 183–193. https://doi.org/10.1016/j.echo.2014.11.003 (2015).
7. Bogunovic, N. et al. Multi-parametric speckle tracking analyses to characterize cardiac amyloidosis: a comparative study of systolic left ventricular longitudinal myocardial mechanics. *Heart Vessels.* **37**, 1526–1540. https://doi.org/10.1007/s00380-022-02047-6 (2022).
8. Pagourelias, E. D. et al. Echo parameters for differential diagnosis in cardiac amyloidosis: a head-to-head comparison of deformation and nondeformation parameters. *Circ. Cardiovasc. Imaging.* **10**, e005588. https://doi.org/10.1161/CIRCIMAGING.116.005588 (2017).
9. Donal, E. & Schnell, F. Mechanical dispersion: the simple, robust parameter we are looking for? Value for the hypertrophic cardiomyopathies. *Eur. Heart J. Cardiovasc. Imaging.* **17**, 622–623. https://doi.org/10.1093/ehjci/jew020 (2016).
10. Holcman, K. et al. Pre-symptomatic scintigraphic and genetic cascade screening in cardiac transthyretin amyloidosis. *Eur. J. Nucl. Med. Mol. Imaging*. https://doi.org/10.1007/s00259-024-06966-6 (2024).
11. Garcia-Pavia, P. et al. Diagnosis and treatment of cardiac amyloidosis: a position statement of the ESC working group on myocardial and pericardial diseases. *Eur. Heart J.* **42**, 1554–1568. https://doi.org/10.1093/eurheartj/ehab072 (2021).
12. Gillmore, J. D. et al. Nonbiopsy diagnosis of cardiac transthyretin amyloidosis. *Circulation* **133**, 2404–2412. https://doi.org/10.1161/CIRCULATIONAHA.116.021612 (2016).
13. Lang, R. M. et al. Recommendations for cardiac chamber quantification by echocardiography in adults: an update from the American society of echocardiography and the European association of cardiovascular imaging. *J. Am. Soc. Echocardiogr.* **28**, 1–39e14. https://doi.org/10.1016/j.echo.2014.10.003 (2015).
14. Phelan, D. et al. Relative apical sparing of longitudinal strain using two-dimensional speckle-tracking echocardiography is both sensitive and specific for the diagnosis of cardiac amyloidosis. *Heart* **98**, 1442–1448. https://doi.org/10.1136/heartjnl-2012-302353 (2012).
15. Mada, R. O. et al. How to define end-diastole and end-systole? Impact of timing on strain measurements. *JACC Cardiovasc. Imaging.* **8**, 148–157. https://doi.org/10.1016/j.jcmg.2014.10.010 (2015).
16. Haaland, T. F. et al. Strain echocardiography is related to fibrosis and ventricular arrhythmias in hypertrophic cardiomyopathy. *Eur. Heart J. Cardiovasc. Imaging.* **17**, 613–621. https://doi.org/10.1093/ehjci/jew005 (2016).

17. Maurer, M. S. et al. Expert consensus recommendations for the suspicion and diagnosis of transthyretin cardiac amyloidosis. *Circ. Heart Fail.* **12**, e006075. https://doi.org/10.1161/CIRCHEARTFAILURE.119.006075 (2019).
18. Holcman, K. et al. The scintigraphic diagnosis of cardiac amyloidosis. An expert opinion endorsed by the section of nuclear medicine of the Polish cardiac society and the Polish nuclear medicine society. *Nucl. Med. Rev. Cent. East. Eur.* **25**, 142–147. https://doi.org/10.5603/NMR.a2022.0033 (2022).
19. Perugini, E. et al. Noninvasive etiologic diagnosis of cardiac amyloidosis using 99mTc-3,3-diphosphono-1,2-propanodicarboxylic acid scintigraphy. *J. Am. Coll. Cardiol.* **46**, 1076–1084. https://doi.org/10.1016/j.jacc.2005.05.073 (2005).
20. Karhan, A. N. et al. Assessment of cardiac function and electrocardiographic findings in patients with wilson's disease. *Cardiol. Young.* **29**, 1183–1188. https://doi.org/10.1017/S104795111900180X (2019).
21. Sperry, B. W. et al. Regional variation in technetium pyrophosphate uptake in transthyretin cardiac amyloidosis and impact on mortality. *JACC Cardiovasc. Imaging.* **11**, 234–242. https://doi.org/10.1016/j.jcmg.2017.06.020 (2018).
22. Leung, S., Leungsuwan, K., Abdel-Latif, A. & Wenk, J. F. Regional end-systolic circumferential strain demonstrates reduced function in remote myocardium after anterior STEMI. *ArXiv* https://doi.org/10.48550/arxiv.2410.01075 (2024).
23. Candan, O. et al. Mechanical dispersion and global longitudinal strain by speckle tracking echocardiography: predictors of appropriate implantable cardioverter defibrillator therapy in hypertrophic cardiomyopathy. *Echocardiography* **34**, 835–842. https://doi.org/10.1111/echo.13547 (2017).
24. Nerbonne, J. M. & Kass, R. S. Molecular physiology of cardiac repolarization. *Physiol. Rev.* **85**, 1205–1253. https://doi.org/10.1152/physrev.00002.2005 (2005).
25. Banasik, G. et al. LV mechanical dispersion as a predictor of ventricular arrhythmia in patients with advanced systolic heart failure: a pilot study. *Herz* **41**, 599–604. https://doi.org/10.1007/s00059-015-4398-9 (2016).
26. Jalanko, M. et al. Left ventricular mechanical dispersion is associated with nonsustained ventricular tachycardia in hypertrophic cardiomyopathy. *Ann. Med.* **48**, 417–427. https://doi.org/10.1080/07853890.2016.1186826 (2016).
27. Ermakov, S. et al. Left ventricular mechanical dispersion predicts arrhythmic risk in mitral valve prolapse. *Heart* **105**, 1063–1069. https://doi.org/10.1136/heartjnl-2018-314269 (2019).
28. Prihadi, E. A. et al. Determinants and prognostic implications of left ventricular mechanical dispersion in aortic stenosis. *Eur. Heart J. Cardiovasc. Imaging.* **20**, 740–748. https://doi.org/10.1093/ehjci/jez004 (2019).
29. Schwarting, S. K. et al. RV-PA uncoupling is associated with increased mortality in transthyretin amyloid cardiomyopathy treated with Tafamidis. *Clin. Res. Cardiol.* https://doi.org/10.1007/s00392-024-02576-2 (2024).
30. Mattig, I. et al. Right heart and left atrial strain to differentiate cardiac amyloidosis and Fabry disease. *Sci. Rep.* **14**, 2445. https://doi.org/10.1038/s41598-024-52890-y (2024).
31. Aimo, A. et al. Assessing cardiac mechanics through left ventricular haemodynamic forces. *Eur. Heart J. Imaging Methods Pract.* **2**, qyae077. https://doi.org/10.1093/ehjimp/qyae077 (2024).

Author contributions
Each author has contributed significantly to the submitted work, including all of the following: (1) conception and design or analysis and interpretation of data (2) drafting of the manuscript or revising it critically for important intellectual content; (3) final approval of the manuscript submitted.

Funding
Pfizer Research Grant: ID#57165999. Research publication fee (Article Processing Charge) supported by Pfizer Polska sp. z o.o.

Declarations

Competing interests
The authors declare no competing interests.

Additional information
Correspondence and requests for materials should be addressed to K.H.

Reprints and permissions information is available at www.nature.com/reprints.

Publisher's Note Springer Nature remains neutral with regard to jurisdictional claims in published maps and institutional affiliations.